

Signal demodulator based on in-phase and quadrature interference-robust feature

Wen Deng¹, XIN CAI², Xiang Wang¹, and Zhitao Huang¹

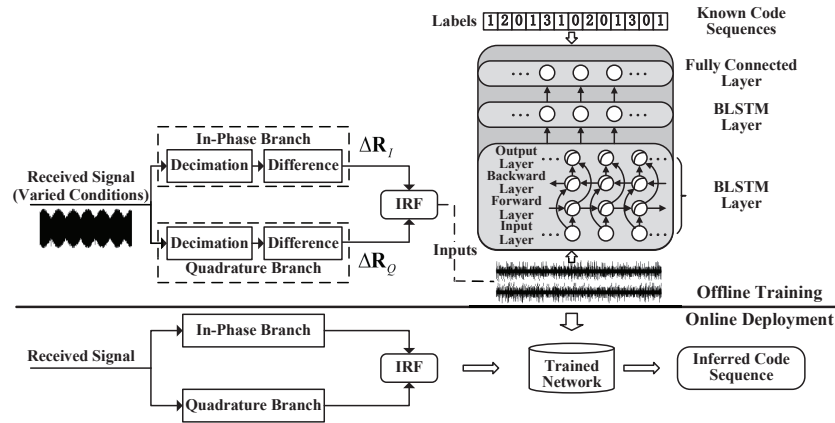
¹National University of Defense Technology

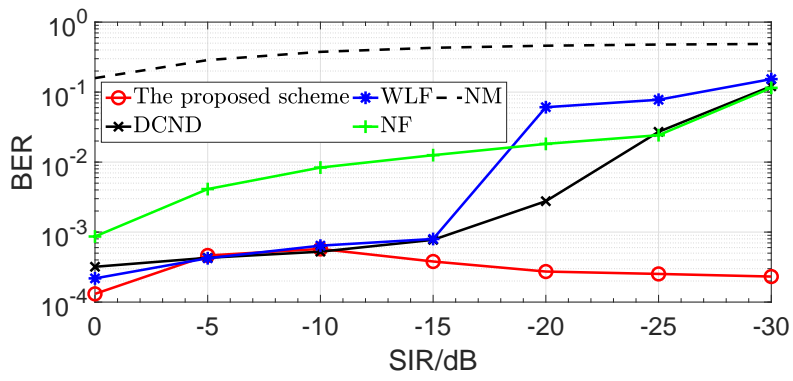
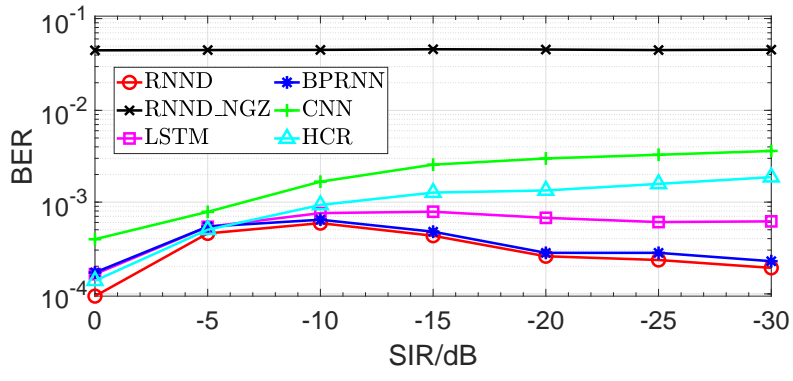
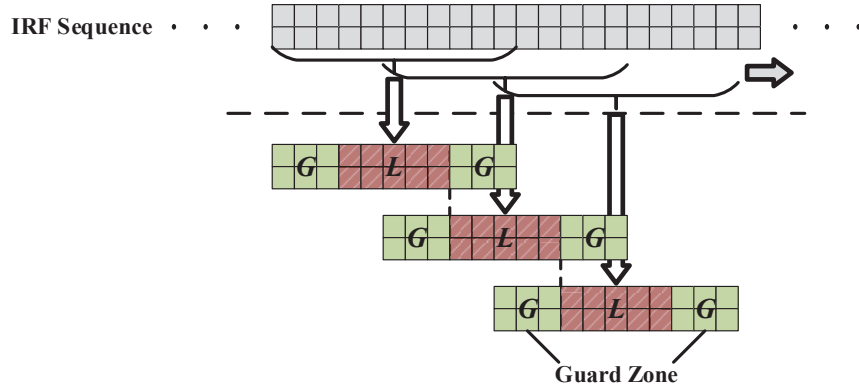
²Academy of Military Science of the People’s Liberation Army

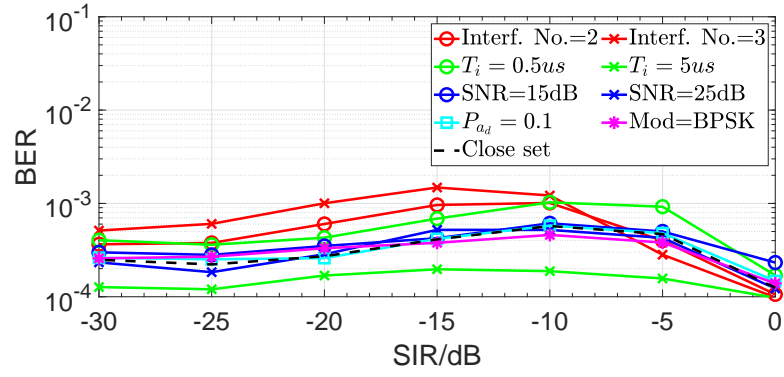
October 24, 2022

Abstract

In this letter, the issue of mitigating strong co-channel interference (CCI) in communication systems is addressed. Unlike conventional model-based methods, a novel data-driven scheme is proposed. A recurrent neural network (RNN) is trained to directly demodulate the desired signal under strong CCI. Instead of inputting the original received signal, in-phase and quadrature interference-robust features (IRF) are extracted through preprocess. The RNN is then trained offline to implement sequence labelling, with the IRF sequences and known code sequences of the desired signal as inputs and ground-truth labels. Meanwhile, a guard zone is introduced when loading the IRF sequences to enable better contextual information exploitation by the RNN demodulator. Online tests validated the low bit error rate (BER) of the RNN demodulator, under strong CCI. Moreover, the proposed scheme outperformed existing model-based and data-driven interference mitigation schemes in terms of the BER, especially in low signal-to-interference ratio region. Inspiringly, the proposed data-driven scheme generalized well to varied unseen test conditions.







Signal demodulator based on in-phase and quadrature interference-robust feature

WEN DENG, Xin CAI, Xiang WANG and Zhitao HUANG

In this letter, the issue of mitigating strong co-channel interference (CCI) in communication systems is addressed. Unlike conventional model-based methods, a novel data-driven scheme is proposed. A recurrent neural network (RNN) is trained to directly demodulate the desired signal under strong CCI. Instead of inputting the original received signal, in-phase and quadrature interference-robust features (IRF) are extracted through preprocess. The RNN is then trained offline to implement sequence labelling, with the IRF sequences and known code sequences of the desired signal as inputs and ground-truth labels. Meanwhile, a guard zone is introduced when loading the IRF sequences to enable better contextual information exploitation by the RNN demodulator. Online tests validated the low bit error rate (BER) of the RNN demodulator, under strong CCI. Moreover, the proposed scheme outperformed existing model-based and data-driven interference mitigation schemes in terms of the BER, especially in low signal-to-interference ratio region. Inspiringly, the proposed data-driven scheme generalized well to varied unseen test conditions.

Introduction: The strong co-channel interference (CCI) issue among coexisting communication systems has attracted widespread attention. For instance, in ultra low power[1] and spread-spectrum overlay systems (e.g., 3G systems sharing the spectrum with existing services)[2], the power of the narrow band interferences could exceed significantly the desired signal power, leading to severe performance degradation

Existing remedial CCI mitigation schemes are basically model-based. For single-receiver systems, typical solutions include the analog/digital notch filters (NF) that introduce spectral nulls at the CCI band [3] and the widely linear filters (WLF) that extract the desired signal based on its cyclostationarity [4]. However, the performance of above schemes deteriorates remarkably when the CCI is significantly stronger than the desired signal. Recently, the application of deep learning (DL) in the communication field has attracted rising interest. In [5], the authors proposed to demodulate mutually-interfering signals via a deep convolutional network demodulator (DCND) and end-to-end training (i.e., with the original single-channel received signal as the network input). The DCND outperformed the conventional correlation demodulation by the anti-interference capability and provided a universal demodulation framework for varied signal patterns.

In this letter, a novel data-driven scheme is proposed for strong CCI mitigation in single-receiver systems. Inspired by the pioneer work in [5], demodulation of the corrupted desired signal is formulated as a sequence labelling task. Since the recurrent neural network (RNN) has been applied widely to solve the sequence labelling problem, we propose to implement the task via a RNN demodulator (RNND). Instead of directly inputting the received signal, in-phase and quadrature interference-robust features (IRF) are first extracted. In the offline training, a RNN is trained with the IRF sequences and known code sequences as the inputs and the ground-truth labels. In the online deployment, the IRF sequence of the received signal is loaded into the trained RNN to infer the code sequence of the desired signal. Meanwhile, to better exploit the context in the RNN inputs, a ‘guard zone’(GZ) is introduced when loading the IRF sequences.

Numerical results validated the low bit-error rates (BER) of the proposed RNND, under strong CCI. Alternative network structures were compared to verify the superiority of the chosen RNN structure. Moreover, the RNND outperformed existing model-based and data-driven interference mitigation schemes, especially in low signal-to-interference ratio (SIR) region. Inspiringly, the proposed data-driven scheme generalized well to varied unseen test conditions.

System Model: Suppose that at the receiving end, a narrow-band CCI $i(t)$ is superimposed on the desired signal $d(t)$, resulting in

$$r(t) = a_d d(t - \tau_d) + a_i i(t - \tau_i) + n(t), t \in [0, T] \quad (1)$$

where a_d and a_i are the channel gain coefficients, τ_d and τ_i are the transmission delays, the subscript ‘ d ’ and ‘ i ’ indicate respectively the desired signal and the interference hereafter. $n(t)$ is the additive white Gaussian noise (AWGN), T is the observation duration. $d(t)$ and $i(t)$ can

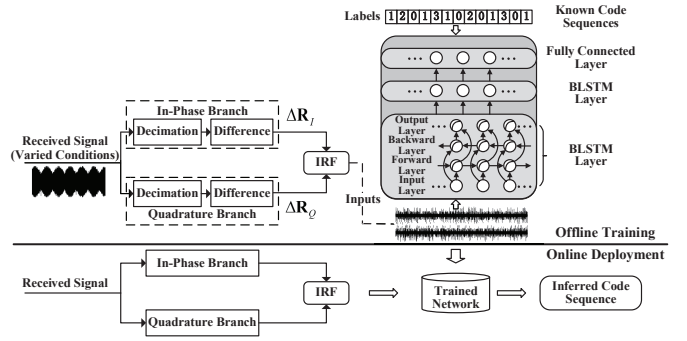


Fig. 1. Schematics of the proposed RNND.

be expressed as

$$d(t) = \sum_{m_d=1}^{M_d} (A_{dc}^{m_d} \cos 2\pi F^c t - A_{ds}^{m_d} \sin 2\pi F^c t) g_d[t - (m_d - 1)T_d] \quad (2)$$

$$i(t) = \sum_{m_i=1}^{M_i} (A_{ic}^{m_i} \cos 2\pi F^c t - A_{is}^{m_i} \sin 2\pi F^c t) g_i[t - (m_i - 1)T_i] \quad (3)$$

where $A_{dc}^{m_d}$ and $A_{ds}^{m_d}$ are respectively amplitudes of the in-phase and quadrature carriers of $d(t)$ when transmitting its m_d th symbol, $A_{ic}^{m_i}$ and $A_{is}^{m_i}$ are amplitudes of the in-phase and quadrature carriers of $i(t)$ when transmitting its m_i th symbol. F^c is the shared carrier frequency. T_d and T_i are the symbol durations. $g_d(t)$ and $g_i(t)$ are the energy-normalized shaping pulses lasting for T_d and T_i respectively. M_d and M_i are the total numbers of symbols. Here, integer number of carrier periods is presumed within one symbol of $d(t)$, i.e., $T_d F^c = k_d \in \mathbb{N}$ (Without loss of generality, we consider k_d even in the following derivations, while similar results can be obtained for an odd k_d). Meanwhile, since the narrow-band interference is considered in this letter, we suppose that $T_d \ll T_i$.

IRF Extraction: Assume perfect synchronization with the desired signal, we propose to first sample $r(t)$ at following instants:

$$t_{m_d} = \frac{T_d}{2} (2m_d - 1) + \tau_d, m_d \in [1, M_d] \quad (4)$$

Let $\mathbf{R}_I \in \mathbb{R}^{1 \times M_d}$ denote the corresponding sample vector, then according to Eqs. (1)(2)(3), the m_d th element of \mathbf{R}_I would be

$$\begin{aligned} \mathbf{R}_I[m_d] = & a_d A_{dc}^{m_d} g_d(T_d/2) + a_i [A_{ic}^{m_i, m_d} \cos 2\pi F^c (t_{m_d} - \tau_i) \\ & - A_{is}^{m_i, m_d} \sin 2\pi F^c (t_{m_d} - \tau_i)] g_i[t_{m_d} - (m_{i, m_d} - 1) \\ & T_i - \tau_i] + n(t_{m_d}), m_d \in [1, M_d] \end{aligned} \quad (5)$$

where we suppose that the m_{i, m_d} th symbol of $i(t)$ is received at t_{m_d} . Eq.(5) is obtained with $\sin 2\pi F^c (t_{m_d} - \tau_d) = 0$ and $\cos 2\pi F^c (t_{m_d} - \tau_d) = 1$. Notice that with $T_d \ll T_i$, $m_{i, m_d+1} = m_{i, m_d}$ for the overwhelming majority of $m_d \in [1, M_d - 1]$. To simplify the analysis, we set aside the few exceptions where $m_{i, m_d+1} \neq m_{i, m_d}$ temporarily, then the 1st-order difference of \mathbf{R}_I can be obtained as

$$\begin{aligned} \Delta \mathbf{R}_I[m_d] = & a_d g_d(T_d/2) (A_{dc}^{m_d+1} - A_{dc}^{m_d}) + a_i \Delta g_i^{m_d+1, m_d} \\ & [A_{ic}^{m_i, m_d} \cos 2\pi F^c (t_{m_d} - \tau_i) - A_{is}^{m_i, m_d} \sin 2\pi F^c \\ & (t_{m_d} - \tau_i)] + [n(t_{m_d+1}) - n(t_{m_d})], m_d \in [1, M_d - 1] \end{aligned} \quad (6)$$

where $\Delta g_i^{m_d+1, m_d}$ is short for $g_i[t_{m_d+1} - (m_{i, m_d} - 1)T_i - \tau_i] - g_i[t_{m_d} - (m_{i, m_d} - 1)T_i - \tau_i]$. Eq.(6) is obtained with $A_{ic}^{m_i, m_d+1} \cos 2\pi F^c (t_{m_d+1} - \tau_i) = A_{ic}^{m_i, m_d} \cos[2\pi F^c (t_{m_d} - \tau_i) + 2\pi k_d] = A_{ic}^{m_i, m_d} \cos 2\pi F^c (t_{m_d} - \tau_i)$ and similarly, $A_{is}^{m_i, m_d+1} \sin 2\pi F^c (t_{m_d+1} - \tau_i) = A_{is}^{m_i, m_d} \sin 2\pi F^c (t_{m_d} - \tau_i)$. Notice that the first and second items in Eq. (6) correspond respectively to the desired signal and the interference.

After mathematical derivations, the average SIR promotion of $\Delta \mathbf{R}_I$ ($\text{SIR}_{\Delta \mathbf{R}_I}$) over $r(t)$ ($\text{SIR}_{r(t)}$) is obtained as

$$\eta_I = \frac{\text{SIR}_{\Delta \mathbf{R}_I}}{\text{SIR}_{r(t)}} \approx \frac{2T_d[g_d(T_d/2)]^2}{T_i(m_{\Delta g_i})^2} \quad (7)$$

where $m_{\Delta g_i}$ denotes the average of $\Delta g_i^{m_d+1, m_d}$ over $m_d \in [1, M_d - 1]$. Eq.(7) shows that the SIR promotion is determined by the ratio between symbol durations of the desired signal and the interference, as well as their shaping pulses. For instance, with $T_d/T_i = 10^{-2}$, and both $g_d(t)$ and $g_i(t)$ being square-root raised cosine windows with roll-off factors 0.5, η_I could theoretically exceed 40dB. When taking the cases where $m_{i, m_d+1} \neq m_{i, m_d}$ into account, a general promotion of over 25dB could still be expected, based on our simulations. Hence, through decimation and difference, information on the amplitudes of the in-phase carrier of the desired signal is extracted in an interference-robust meanwhile context-dependent manner (i.e., the first part of Eq.(6)).

On the other hand, we may re-sample $r(t)$ at following instants:

$$t'_{m_d} = \frac{T_d}{2} (2m_d - 1 - \frac{1}{2k_d}) + \tau_d, m_d \in [1, M_d] \quad (8)$$

After taking the 1st-order difference of the sample vector, the quadrature counterpart of the desired signal can be extracted as

$$\begin{aligned} \Delta \mathbf{R}_Q[m_d] = & a_d g_d(T_d/2 - \frac{T_d}{4k_d})(A_{ds}^{m_d+1} - A_{ds}^{m_d}) + a_i \Delta' g_i^{m_d+1, m_d} \\ & [A_{ic}^{m_i, m_d} \cos 2\pi F^c(t'_{m_d} - \tau_i) - A_{is}^{m_i, m_d} \sin 2\pi F^c(t'_{m_d} \\ & - \tau_i)] + [n(t'_{m_d+1}) - n(t'_{m_d})], m_d \in [1, M_d - 1] \end{aligned} \quad (9)$$

where $\Delta' g_i^{m_d+1, m_d}$ is short for $g_i[t'_{m_d+1} - (m_i, m_d - 1)T_i - \tau_i] - g_i[t'_{m_d} - (m_i, m_d - 1)T_i - \tau_i]$. Similar to $\Delta \mathbf{R}_I$, power of the interference is also remarkably suppressed in $\Delta \mathbf{R}_Q$.

In this letter, $\Delta \mathbf{R}_I$ and $\Delta \mathbf{R}_Q$ are stacked to form the IRF sequence of $r(t)$ as follow:

$$\mathbf{IRF} = \begin{bmatrix} \Delta \mathbf{R}_I[1] & \cdots & \Delta \mathbf{R}_I[m_d] & \cdots & \Delta \mathbf{R}_I[M_d - 1] \\ \Delta \mathbf{R}_Q[1] & \cdots & \Delta \mathbf{R}_Q[m_d] & \cdots & \Delta \mathbf{R}_Q[M_d - 1] \end{bmatrix} \quad (10)$$

RNN-based sequence labelling: Unlike the standard feedforward neural network, the RNN retains a state representing information from a context window, and thus can model dependence among input and/or output[6]. Hence, the RNN has been applied successfully in varied sequence learning tasks, including sequence labelling, among others. Sequence labelling implements the task of assigning sequences of labels, drawn from a fixed alphabet, to sequences of input data [7]. Let S be a set of training samples drawn from a fixed distribution $\mathcal{D}_{\mathcal{X} \times \mathcal{Z}}$. The input space $\mathcal{X} = (\mathbb{R}^M)^*$ is the set of all sequences of size M real-valued vectors. The target space $\mathcal{Z} = L^*$ is the set of all sequences over the alphabet L of labels. Each element of S is a pair of sequences (\mathbf{x}, \mathbf{z}) . The task is to use S to train a sequence labeller $h: \mathcal{X} \rightarrow \mathcal{Z}$ to label the sequences in a test set $S' \subset \mathcal{D}_{\mathcal{X} \times \mathcal{Z}}$. When carrying out sequence labelling via the RNN, the training can be accomplished by iteratively updating parameters of the network to minimize cross-entropy loss function.

On the other hand, to tackle the deficiencies of the primitive RNN, several remedial architectures have been introduced. The most successful ones include the long short-term memory (LSTM) and the bidirectional structure [8]. The LSTM introduces the memory cell to replace traditional nodes in the hidden layer of the primitive RNN, and thus enables the exploitation of long-term contextual information in the input/output. The bidirectional structure consists of two separate recurrent hidden layers operating on the input sequence respectively in backward and forward directions, and thus extends the primitive RNN to model dependence on both past and future states.

RNND Implementation: Fig. 1 illustrates the proposed RNND for CCI mitigation. Demodulation of the desired signal under CCI is formulated as a sequence labelling task, which is implemented by a multi-layer RNN. The input space $\mathcal{X} = (\mathbb{R}^2)^*$ is the set of all IRF sequences. The target space \mathcal{Z} is the set of all possible code sequences of the desired signal. In the offline training, the IRF sequences are extracted under varied conditions. The corresponding known code sequences of the desired signal act as the ground-truth labels to compute the loss function at the output end of the RNN. Specifically, for each training sample, the

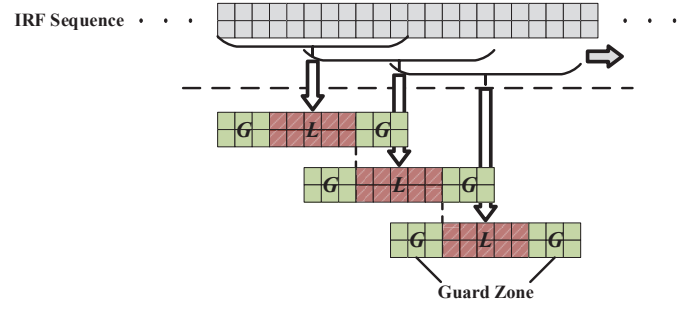


Fig. 2. Segmentation of the IRF sequence with the GZ.

label corresponding to the input vector $\mathbf{IRF}[m_d]$ is the m_d th code of the desired signal. In the online deployment, the IRF sequence extracted from the received signal under test is loaded into the trained RNN. The output of the network is then the inferred code sequence of the desired signal. The multi-layer RNN consists of two bidirectional LSTM (BLSTM) layers and one fully connected linear layer, with Softmax activation function. The output dimension of the fully connected layer is determined by the modulation order of the desired signal.

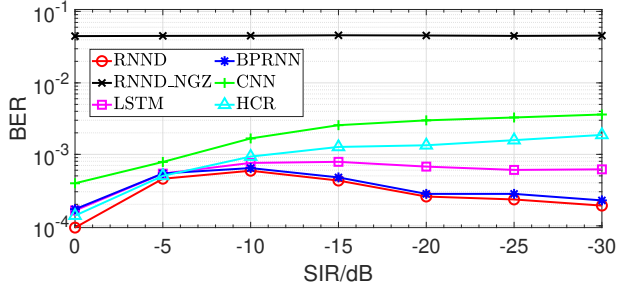
In both training and test, the IRF sequences need to be segmented into blocks of equal length before being loaded separately into the network. However, one main drawback of segmenting by consecutive non-overlapping windows is that it hinders the BLSTM layers from accessing to bidirectional contexts when modelling elements on the border of each block. For such elements, either the past or future contextual information would be insufficient. To overcome this limitation, we propose to segment the IRF sequences by overlapped windows with GZ. Fig. 2 illustrates how the IRF sequence is segmented with the GZ. The total length of the segmentation window is $L + 2G$, with guard zones of length G at both ends of each block. After segmenting one block, the window is shifted by L to the next block. Note that in both offline training and online deployment, only the outputs corresponding to the $[G + 1, G + L]$ th elements of each block are considered in the loss computation and as the inferred codes, i.e., the outputs corresponding to the GZ are discarded. Existence of the GZ ensures that all elements are given sufficient contextual information when being modelled.

Numerical Results: Basic experiment setup is listed in Table 1. After training, the proposed RNND was tested under varied interference intensities. Meanwhile, the performance of various alternative network structures was compared. These included the LSTM layers, the bidirectional primitive recurrent layers, the convolutional layers, the hybrid convolutional&recurrent layers and the fully connected layers (corresponding networks were denoted respectively as the ‘LSTM’, ‘BPRNN’, ‘CNN’, ‘HCR’ and ‘FC’). Moreover, to testify the effect of introducing the GZ, we also set the GZ length to be 0 for comparison (denoted as the ‘RNND_NGZ’). Fig. 3 demonstrates the test BER of above structures under varied SIR. It can be seen that the proposed RNND accurately demodulated the desired signal under CCI of varied intensities, even for SIR as low as -30dB. Meanwhile, it outperformed all other structures under each SIR tested, especially in low SIR region. The poor performance of the RNND_NGZ validated the necessity of the GZ. The superiority of the RNND with BLSTM layers over the LSTM and the BPRNN indicated that bidirectional and long-term contextual information was essential to the current sequence labelling task. Exploitation of such sophisticated dependence was necessitated by the differential operation in the IRF extraction. Results of the CNN and the HCR indicated that recurrent structures were more effective than convolutional ones in modelling the intrinsic sequential structures of inputs and outputs herein.

Next, the proposed RNND was compared with existing interference mitigation schemes, including data-driven (DCND) and model-based (WLF, NF) ones. The results are demonstrated in Fig. 4. The theoretical BER with no interference mitigation is also given (denoted as ‘NM’). We can see that, as the received signal was loaded directly into the DCND, without interference-suppressive preprocess, its performance deteriorated remarkably under strong CCI ($\text{SIR} \leq -20\text{dB}$). This was also the case for the WLF and NF, the BER of which rose remarkably as the SIR dropped below -15dB. In contrast, the RNND performed robustly in low SIR region. This should mainly be attributed to the IRF extraction and the

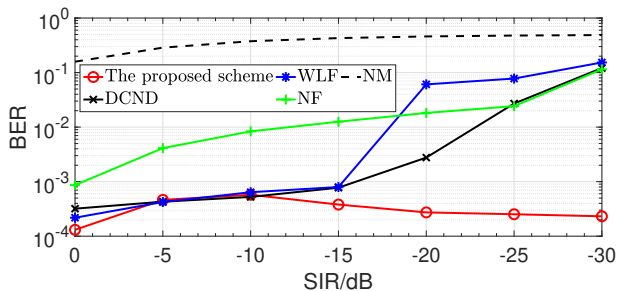
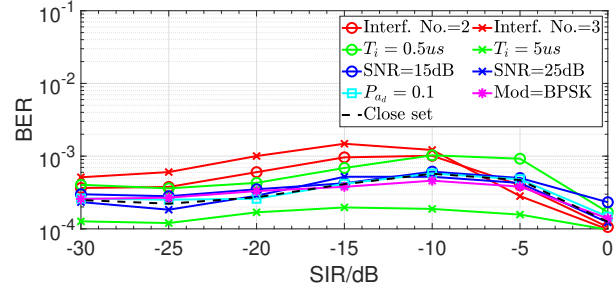
Table 1: Basic experiment setup

Parameters	Values/Settings
Parameters of $d(t)$	QPSK, $F^c=4\text{GHz}$, $T_d=1\text{ns}$, $g_d(t)$:square root raised cosine, roll-off:0.5
Parameters of $i(t)$	QPSK, $F^c=4\text{GHz}$, $T_i=1\text{us}$, $g_i(t)$:square root raised cosine, roll-off:0.5
SIR	[0, -5, -10, -15, -20, -25, -30]dB
SNR	20dB
Training/Validation/Test sets	$M_d=10^5, 2 \times 10^4, 10^6$ per SIR
Neurons per hidden layer	128
Guard zone length	5
Batchsize	200
Training optimizer/Learning rate	Adam, 0.001
Training epoches	200

**Fig. 3** Test BER of the RNND and alternative network structures under varied SIR.

edges that connect adjacent time steps in the RNN nodes [6]. Since in the IRF sequences, the interference component was remarkably suppressed for $\{m_d|m_{i,m_d+1}=m_{i,m_d}\}$, the BER performance of the RNND depended mainly on the distorted IRF points (i.e., $\{m_d|m_{i,m_d+1} \neq m_{i,m_d}\}$ where the interference component was non-negligible). Luckily, with the edges connecting adjacent time steps, the output of the RNN at each time step was calculated based on both the current input and the contextual states. Hence, once the RNN had learnt to distinguish between the distorted and normal IRF points, it may adjust the weights to rely more on contextual states in case of the former. Notice that the BER of the RNND peaked at SIR=-10dB rather than intuitively at SIR=-30dB. This was because the lower the SIR was, the more distinguishable the distorted and normal IRF points were, as found in our simulations. For intermediate SIR ($[0 \sim -10]$ dB), the distorted IRF points were of close amplitudes with the normal ones. It would be more likely for the RNN to treat the distorted inputs directly as the normal ones, without necessary weight adjustment.

The generalization capability is crucial for data-driven schemes to be practical, i.e., whether the trained scheme can cope with unseen test conditions. Since the interference and environmental parameters could be unknown in practice, we further tested the RNND under generalized conditions. Specifically, the number ('Interf. No.=2, 3'), symbol duration ($T_i=0.5\text{us}, 5\text{us}$) and modulation pattern ('Mod=BPSK') of the interference were respectively changed. We also tested the cases where the SNR ('SNR=15dB, 25dB') varied or a_d was randomly perturbed by certain ratio ($a_d = a_d + \text{random}(-1, 1) \cdot P_{a_d}$, $P_{a_d} = 0.1$). Fig. 5 demonstrates the generalization performance of the RNND. It can be seen that the RNND coped well with all tested unseen conditions. The inspiring generalization capability in the interference parameters should mainly be attributed to the IRF extraction, which made the scheme less

**Fig. 4** Test BER of different interference mitigation schemes under varied SIR.**Fig. 5** BER of the RNND under generalized test conditions.

interference-sensitive. On the other hand, the BER increased slightly as the interference number rose or T_i dropped, mainly due to the increase of distorted IRF points.

Conclusions: A data-driven CCI mitigation scheme is proposed. The corrupted desired signal is demodulated by a RNND, in the form of sequence labelling. Close and open set tests validated the effectiveness of the RNND in low SIR region and its generalization capability. The RNND outperformed existing model-based/data-driven interference mitigation schemes in terms of the BER, especially under strong CCI. Future work may focus on extending the scheme towards wideband interference scenarios where as T_d/T_i rises, the current IRF would be less effective in interference suppressing. Hence, the design of novel network inputs is necessitated.

Wen DENG, Xin CAI, Xiang WANG, Zhitao HUANGJ (*National University of Defense Technology, China*)

E-mail: williamxman@163.com

A. Xin CAI (*Academy of Military Science of the People's Liberation Army, China*)

References

- N. F. Kiyani, V. Sridharan, and G. Dolmans, "Co-channel interference mitigation technique for non-coherent OOK receivers," *IEEE Wireless Communications Letters*, vol. 3, no. 2, pp. 189–192, 2014.
- H. V. Poor, "Active interference suppression in CDMA overlay systems," *IEEE J.Select.Areas in Commun*, vol. 19, no. 1, pp. 4–20, 2001.
- H. Shaman and J. S. Hong, "Ultra-wideband (UWB) bandpass filter with embedded band notch structures," *IEEE Microwave and Wireless Components Letters*, vol. 17, no. 3, pp. 193–195, 2007.
- P. Chevalier, R. Chauvat, and J. P. Delmas, "Enhanced widely linear filtering to make quasi-rectilinear signals almost equivalent to rectilinear ones for SAIC/MAIC," *IEEE Transactions on Signal Processing*, vol. 66, no. 6, pp. 1438–1453, 2017.
- X. Lin, R. Liu, W. Hu, Y. Li, X. Zhou, and X. He, "A deep convolutional network demodulator for mixed signals with different modulation types," in *IEEE Int. Conf. on Big Data Intelligence, Computing, Cyber Science and Technology Congress*, pp. 893–896, 2017.
- L. Zachary, B. John, and E. Charles, "A critical review of recurrent neural networks for sequence learning," *arXiv:1506.00019*, 2015.
- G. Alex, *Supervised sequence labelling with recurrent neural networks*. Springer-Verlag Berlin Heidelberg, 2012.[Online]. Available: <http://www.cs.toronto.edu/graves/preprint.pdf>.
- M. Schuster and K. K. Paliwal, "Bidirectional recurrent neural networks," *IEEE Transactions on Signal Processing*, vol. 45, no. 11, pp. 2673–2681, 1997.